cover the same λ_{III} range; moreover, the ultraviolet spacings at the extreme hour angles give the north-south resolution and have the appropriate spatial scales to record the major structures of Jupiter's radiation belts. The λ_{III} assigned to the images is therefore that of the extreme hour angles. The difference between the images of 15 and 20 July reflects the changes that occurred to the range longitudes to which the instrument is sensitive. The left side of the belt is much brighter than the right side. This agrees with the sequence of VLA images taken on 19 and 20 July (by I. de Pater *et al.*, in preparation). The AT images are reported by Y. Leblanc and G. A. Dulk, *Geophys. Res. Lett.*, in press; G. A. Dulk, Y. Leblanc, R. W. Hunstead, *ibid.*, in press.

18. J. H. Waite Jr. *et al.*, *Science*, in press; J. T. Clarke *et al.*, *ibid.* **267**, 1302 (1995).
19. N. M. Brice and T. R. McDonough, *Icarus* **18**, 206 (1973).
20. I. de Pater and C. K. Goertz, *J. Geophys. Res.* **99**, 2271 (1994).
21. W.-H. Ip, *Eos* **75** (fall suppl.), 404 (1994); *Planet. Space Sci.*, in press; A. J. Dessler and T. W. Hill, *Bull. Am. Astron. Soc.* **26**, 1593 (1994); T. Hill and A. J. Dessler, *Eos* **75** (fall suppl.), 402 (1994).
22. I. de Pater, *Astron. J.* **102**, 795 (1991).
23. S. J. Bolton, M. J. Klein, S. Gulkis, R. M. Thorne, R. Foster, *Eos* **75** (fall suppl.), 405 (1994).
24. S. H. Brecht, M. E. Pesses, J. G. Lyon, N. T. Gladd, S. W. McDonald, *Geophys. Res. Lett.*, in press; S. H. Brecht, M. E. Pesses, I. de Pater, N. T. Gladd, J. G. Lyon, *ibid.*, in press.
25. M. Horanyi, *ibid.* **21**, 1039 (1994).
26. M. Wong *et al.* in preparation.
27. This research was supported in part by National Science Foundation grant 22122 and National Aeronautics and Space Administration (NASA) grant NAGW-3917 to the University of California, Berkeley. The Westerbork telescope is operated by the Netherlands Foundation for Research Astronomy with financial support from the Netherlands Organization for Scientific Research (NWO). The VLA and the 140-foot telescope at Green Bank are part of the National Radio Astronomy Observatory, which is operated by Associated Universities, Inc., under a cooperative agreement with the National Science Foundation. The AT is operated by the Australia Telescope National Facility, CSIRO. The MOST is supported by grants from the Australian Research Council, the University of Sydney Research Grants Committee, and the Science Foundation for Physics within the University of Sydney. The Naval Research Laboratory's Maryland Point Observatory is supported by the Office of Naval Research and through an interagency agreement with NASA. The Dominion Radio Astrophysics Observatory synthesis telescope is operated by the National Research Council of Canada as a national facility. A portion of the work was performed by the Jet Propulsion Laboratory under contract with NASA.

19 December 1994; accepted 1 May 1995

Observation of Individual Chemical Reactions in Solution

Maryanne M. Collinson* and R. Mark Wightman†

Discrete chemical reaction events occurring in solution have been observed by single photon detection of a bimolecular, chemiluminescent reaction. The reactants were generated from 9,10-diphenylanthracene in acetonitrile with potential pulses applied to an ultramicroelectrode. Electrogenerated radical ions of opposite sign react to yield the excited singlet state of the parent compound. The chemical reactions were restricted to a 20-femtoliter volume adjacent to the electrode by the use of rapid potential pulses. Individual chemical reaction events were stochastic and followed the Poisson distribution, and the interarrival time between successive reaction events was exponentially distributed.

At a microscopic level, bimolecular chemical reactions generate products as a result of the collision of individual molecules. Normally, however, chemical reactions in solution are viewed as an ensemble of events, and the fluctuations associated with individual molecular collisions and their reactions are not observed. This is because both the location and time of an individual reaction event are usually undefined as a result of diffusion and encounter of the reagents before the reaction. In the gas phase, individual reactions can be examined because methods exist for exquisite control of delivery of reactants (*1*). In solids, the immobile nature of individual molecules allow their examination by near-field scanning microscopy (*2*) and laser spectroscopy (*3*). Although such approaches cannot be used for chemical reactions in fluids, we show that single reactions can be observed by restricting the volume occupied by the reactants and the observation time. This approach is similar to that used for solution-phase single molecule detection where molecules are spatially restricted in microdroplets (*4*), a thin flow cell (*5*), or at the focal point of a confocal microscope (*6*), and then temporally interrogated through laser-induced fluorescence (LIF). In this work, the solution reagents are restricted to a microscopic volume by electrogeneration with a microelectrode (*7*). The reagents undergo a chemiluminescent (CL) reaction (*8*) whose photon emission is time resolved with a multichannel scaler. This experiment reveals the stochastic nature of molecular reactions in solution and enables observation of the rates of chemical reactions at the level of individual events.

Introduction of 9,10-diphenylanthracene (DPA) in an acetonitrile solution into an electrochemical cell containing a microelectrode (*9*) pulsed between potentials sufficient to alternately generate its radical cation and radical anion results in chemiluminescence (Fig. 1A). The emission occurs predominantly during the shorter (50 μs) cathodic pulse (Fig. 2) as the electrogenerated radical anion diffuses into the sea of DPA radical cations generated in the 500-μs interval before the cathodic pulse. When the radical ions of opposite charge encounter each other, they react by electron transfer reaction to form either the nonemitting triplet state of DPA or the excited singlet state that relaxes to the ground state by photon emission (*10*). These events occur in a region adjacent to the electrode that has a volume of ~20 femtoliters defined by the electrode area (9×10^{-7} cm^2) and the distance an electrogenerated ion can diffuse from the electrode surface during the 50-μs step.

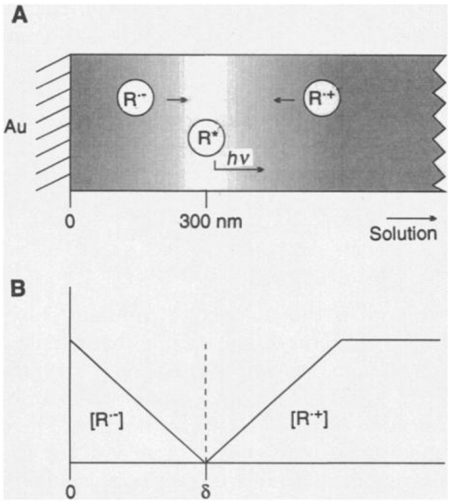

Fig. 1. Schematic diagram of the chemical reaction. (**A**) A radical anion ($R^{\cdot -}$) of 9,10-diphenylanthracene (DPA) is electrogenerated at a gold electrode during the cathodic potential pulse. It diffuses away from the electrode and encounters a radical cation ($R^{\cdot +}$) electrogenerated during the preceding time interval in which the electrode was maintained at a positive potential. The singlet-excited state of DPA (R^{*}) is generated as a result of electron transfer between the two reactants. Photon emission leads to detection of the single chemical reaction. (**B**) Concentration profiles of the reactants for high concentrations of precursor as described by Eq. 2 (see text). Under this condition, the photon emission arises from a sharp plane at the intersection of the concentration profiles located a distance δ from the electrode surface.

When the photons are counted over 1-s intervals, no evidence for individual reaction events is observed. The ensemble av-

---

Department of Chemistry, University of North Carolina, Chapel Hill, NC 27599-3290, USA.

*Present address: Department of Chemistry, Kansas State University, Manhattan, KS 66506-3701, USA.
†To whom correspondence should be addressed.

erage of the counts detected during 1000 cathodic voltage pulses also masks individual reaction events but reveals that the luminescence approaches steady state (Fig. 2D) (*11*). When events during a single cathodic pulse are viewed with greater temporal resolution, photons resulting from individual reactions are resolved (Fig. 2, E and F). Virtually no background photons are detected (*12*) so the corrections required with LIF techniques are unnecessary. Thus, the individual counts (photons) shown in Fig. 2, E and F, result solely from single chemical reactions between individual DPA radical ions in solution.

The stochastic nature of these events was characterized in two ways (Fig. 3). First, a histogram of the time between individual photons was constructed (Fig. 3A). Such a histogram for random events should be an exponential whose frequency (λ) gives the mean rate of the events (*13*). The value of λ from the exponential was in excellent agreement with the mean rate of photon arrival obtained by ensemble averaging data from repetitive cathodic pulses. Second, the data followed a Poisson distribution (Fig. 3B):

$$P_n(t) = e^{-\lambda t}(\lambda t)^n/n! \qquad (1)$$

where n is the number of cathodic pulses evaluated. This distribution is characteristic of discrete, random, independent events (*13*). The value of λ was similar to that obtained in the exponential distribution. These analyses show that the time scale of the measurement is sufficient to reveal individual reactions in the restricted volume used.

The measured value of λ should be a function of the generation rate and diffusion of the radical ions, the rate and efficiency of the light-producing chemical reaction, as well as the photon collection efficiency (*14*). At concentrations greater than 20 μM, λ, normalized by concentration and electrode area, was essentially constant (inset, Fig. 3B). The ratio of the mean photon rate (accounting for the detection efficiency) and the mean rate of generation of radical anions during each cathodic pulse directly yields the probability of a reaction generating a photon (ϕ_{CL}). At the higher concentrations, this ratio yields a value of ϕ_{CL} of 6%, in good agreement with reported values for DPA in acetonitrile (*8*). At lower concentrations, the normalized value of λ decreases (inset, Fig. 3B).

The concentration-dependent behavior can be understood by consideration of the sequential steps that result in light emission. The absolute rate of photon production (dN/dt) is a function of two sequential processes: diffusion of a radical anion from the electrode, and its rate of reaction with an encountered radical cation. At high concentrations, the reaction occurs in a plane at which the concentration of radical ions approach zero (*10*) located between the two concentration gradients of the reactive ions as illustrated in Fig. 1B. The pseudo-steady state nature of the ensemble average of multiple cathodic steps supports the assumption of a constant concentration gradient of length δ for the radical anion from the electrode surface. Thus, the expression for the rate of light production can be written as:

$$1/(dN/dt) = 1/(N_a A \phi_{CL}) \times \{\delta/(D[\mathrm{DPA}]) + 1/(k[\mathrm{DPA}])\} \qquad (2)$$

where A is the emission area, taken as the area of the electrode, D is the diffusion coefficient of the radical anion (1.3×10^{-5} cm^2 s^{-1}), and N_a is Avogadro's number. In this expression, diffusion of the radical cation and its concentration are incorporated in k, the pseudo–first order rate constant for formation of the excited singlet state at the edge of the radical-cation concentration profile. Thus, when diffusion is rate limiting (first term in the brackets), λ should be first order in [DPA] as found at concentrations greater than 20 μM, but a higher order dependence should be obtained as the concentration is lowered and the rate of the chemical reaction becomes rate limiting. The λ values obtained in Fig. 3 at high concentration yield a value for δ of ~300 nm, consistent with the calculated diffusion distance $\delta = (Dt)^{1/2}$, where t is the time of the cathodic pulse (*15*).

With the use of more conventional electrochemical techniques, we previously determined the second-order, homogeneous

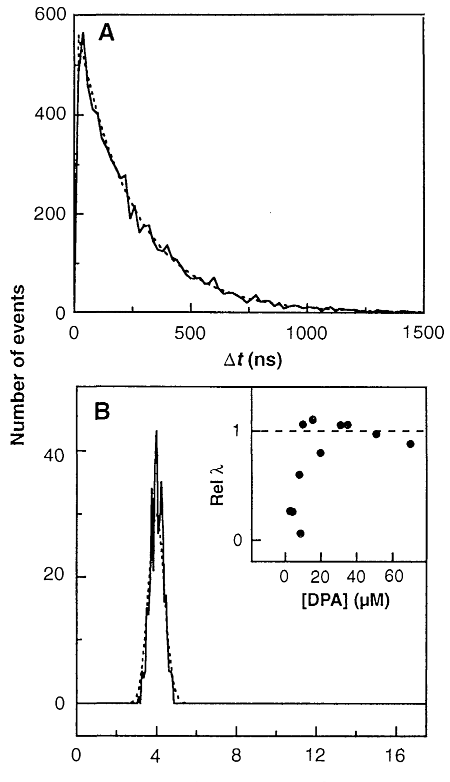

Fig. 3. Poisson description of single reaction events obtained in an acetonitrile solution containing 31 μM DPA. (**A**) Histogram (7000 interevent times and a bin size of 20 ns) of interarrival times and (**B**) histogram (375 voltage pulses and a bin size of 0.8 counts per microsecond). The counts used were from the last 25 μs of the voltage pulse where the emission rate is pseudo–steady state. Dashed line: (A) exponential fit to data with rate of 205 counts per 50 μs and (B) Poisson fit to data with rate of 200 counts per 50 μs. Other conditions as in Fig. 2. Insert: Plot of relative λ values (λ normalized by DPA concentration and electrode area and given as a ratio of the highest value) obtained from Poisson distributions. Data were obtained with electrodes of radii of 5.4 or 2.5 μm.

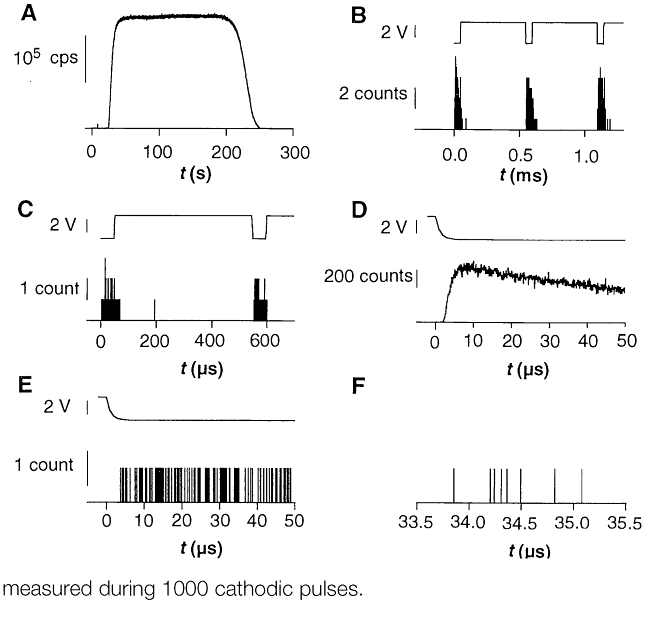

Fig. 2. Temporal resolution of single reaction events. (**A**) Chemiluminescence from a bolus of 15 μM DPA in acetonitrile containing 0.1 M tetrabutylammonium hexafluorophosphate. The electrode was a gold disk (radius = 5.4 μm) pulsed from 1.7 to −2.1 V at 550-μs intervals. Data were collected during the time interval between 50 and 200 s have been expanded through a successive decrease in the bin size from 1 s (A) to 1 μs (**B**), 100 ns (**C** and **D**), and 5 ns (**E** and **F**). The double-layer capacitance (14 pf) and the solution resistance (75 kohm) were used to calculate the rise time of the voltage pulses shown in (D) and (E). The curve shown in (D) is an ensemble average of events measured during 1000 cathodic pulses.

rate constant to be 3×10^9 M^{-1} s^{-1} for the reaction of the oppositely charged radical ions to generate the excited singlet state (*10*). Thus, under more dilute conditions, a radical anion can diffuse some distance into the region where the radical cation exists without reaction, and a sharp reaction zone no longer exists. For example in the presence of 10 μM radical cation, the half life of the reaction will be $\sim$25 μs, and only a portion of the radical anions will react during the 50-μs voltage pulse leading to the lower normalized λ value. Indeed, for concentrations where low values of λ are obtained, the relative number of photons produced after the cathodic pulse increases, which shows that some radical anions fail to react during the pulse. Taken together, the concentration-dependent, stochastic data illustrate the dynamic competition between the rates of diffusion and chemical reaction for a process whose rate constant is near the diffusion-controlled limit.

With sufficient temporal and spatial resolution, all bimolecular chemical reactions should have the stochastic appearance revealed in this work. However, with the exception of measurements of ion fluxes through individual channels in biological membranes (*16*), there are few other examples that so clearly reveal these fundamental events in solution. Most investigations of stochastic events involve the random actions of groups of particles as opposed to the individual events observed here (*17*). For example, the stochastic nature of the electrical noise generated by fluctuations of electrons and ions at the electrode-electrolyte interface (*18*) and the process of electronucleation of multiple atoms during metal deposition on electrodes (*19*) arise from stochastic processes. Indeed, these events for a single molecule have recently been measured with a scanning electrochemical microscope (*20*). In the measurements shown here, however, individual reaction events that can be counted and yet arise from a condition where all of the reagents are freely diffusing solution components.

The ability to observe individual chemical reactions in solution opens many new possibilities for investigation in addition to this new way to determine the rate-limiting step of bimolecular reactions. For example, although the excited singlet lifetime of DPA is too short for resolution in these experi ments, longer lived intermediates in chemiluminescent reactions, such as the excited triplet state of ruthenium trisbipyridine (*21*), should have a lifetime accessible with this technique. With a polychromator, the energy of each individual reaction could be probed. In addition, the Poisson distribution describing the results observed in these experiments defines the standard deviation for this method when used in trace analysis. In all of these applications, the stochastic nature of single reaction events adds a new dimension that can now be probed.

REFERENCES AND NOTES

1. G. Scales, D. Bassi, U. Buck, D. Lainé, Eds., *Atomic and Molecular Beam Methods* (Oxford Univ. Press, Oxford, 1988), vol. 1.
2. R. Kopelman and W. Tan, *Science* **262**, 1382 (1993); E. Betzig and R. J. Chichester, *ibid.*, p. 1422; J. K. Trautman *et al.*, *Nature* **369**, 40 (1994); X. S. Xie and R. C. Dunn, *Science* **265**, 361 (1994); W. P. Ambrose *et al.*, *ibid.*, p. 364.
3. W. E. Moerner, *Science* **265**, 46 (1994).
4. M. D. Barnes, K. C. Ng, W. B. Whitten, J. M. Ramsey, *Anal. Chem.* **65**, 2360 (1993).
5. R. A. Mathies *et al.*, *ibid.* **62**, 1786 (1990); J. Tellinghulsen *et al.*, *ibid.* **66**, 64 (1994).
6. S. Nie *et al.*, *Science* **266**, 1018 (1994).
7. R. M. Wightman, *Science* **240**, 415 (1988); ______ and D. O. Wipf, *Acc. Chem. Res.* **23**, 64 (1990).
8. R. E. Visco and E. A. Chandross, *J. Am. Chem. Soc.* **86**, 5350 (1964); L. R. Faulkner and A. J. Bard, *Electroanalytical Chemistry* A. J. Bard, Ed. (Dekker, New York, 1977), vol. 10, pp. 1–95; F. E. Beideman and D. M. Hercules, *J. Phys. Chem.* **83**, 2203 (1979).
9. The experimental arrangement has been described previously (*10*). The microelectrode was encased in epoxy and formed the floor of an electrochemical cell whose height was 0.15 mm. A photomultiplier tube (Hammamatsu 5600P), attached through a high-speed amplifier to the discriminator of a multichannel scaler, was placed 2 mm from a glass plate that formed the cell top. No lenses were used. Reagents were introduced into the cell with a loop injector with a flow rate of 0.3 ml/min. Potentials are given versus a silver wire pseudo-reference electrode.
10. M. M. Collinson and R. M. Wightman, *Anal. Chem.* **65**, 2576 (1993); M. M. Collinson, P. Pastore, K. M. Maness, R. M. Wightman, *J. Am. Chem. Soc.* **116**, 4095 (1994); M. M. Collinson, P. Pastore, R. M. Wightman, *J. Phys. Chem.* **98**, 11942 (1994).
11. The time-averaged photon emission is pseudo-steady state because the amount of radical cation in solution exceeds the amount of radical anion generated during the cathodic pulse. A steady-state generation rate is desirable to meet the requirement for stationarity necessary for a Poisson distribution.
12. The background in this experiment is negligible on the 50-μs time scale of each voltage pulse and is due to the dark counts of the photomultiplier tube (50/s). A suspected background count is seen at 195 μs in Fig. 2C.
13. N. G. van Kampen, *Stochastic Processes in Physics and Chemistry* (North-Holland, Amsterdam, 1981); S. M. Ross, *Stochastic Processes* (Wiley, New York, 1983).
14. The quantum efficiency of the photomultiplier tube is 0.2, and the efficiency of collection of photons is estimated to be 5% by conventional electrochemical luminescence experiments (*10*).
15. For $\lambda = 205$ counts per 50 μs, 20,500 light-producing reactions occurred. Thus, $dN/dt = 4.1 \times 10^8$ reactions per second.
16. D. Colquhoun and A. G. Hawkes, *Single Channel Recording*, B. Sakmannn and E. Neher, Eds. (Plenum, New York, 1983), pp. 135–188.
17. A. H. W. Beck, *Statistical Mechanics, Fluctuations, and Noise* (Arnold, London, 1976); A. Bezegh and J. Janata, *Anal. Chem.* **59**, 494A (1987).
18. C. Gabrielli, F. Huet, M. Keddam, *J. Chem. Phys.* **99**, 7232 (1993); *ibid.*, p. 7240.
19. P. Bindra, M. Fleischmann, J. W. Oldfield, D. Singleton, *Faraday Discuss. Chem. Soc.* **56**, 180 (1974).
20. F. F. Fan and A. J. Bard, *Science* **267**, 871 (1995).
21. W. L. Wallace and A. J. Bard, *J. Phys. Chem.* **83**, 1350 (1979).
22. Discussions with M. Berkowitz, L. Pedersen, and K. Maness are gratefully acknowledged as is the aid of P. Pastore with simulations of this problem. This work was supported by the National Science Foundation.

8 February 1995; accepted 5 May 1995

Skulls and Anterior Teeth of *Catopithecus* (Primates:Anthropoidea) from the Eocene and Anthropoid Origins

Elwyn L. Simons

Recent finds of *Catopithecus browni* at an upper Eocene fossil site in the Fayum depression, Egypt, reveal features of the earliest higher primates. This basal anthropoidean shows a set of derived cranial and dental features that first occur in combination in this fossil. Old World Anthropoidea or Catarrhini can now be traced back to *Catopithecus* in Egypt. Size, shape, orientation of incisors and canines, and other features of the teeth and skull relate *Catopithecus* both to later Anthropoidea and to the early and middle Eocene cercamoniine adapoids. Most defining characteristics of higher primates cannot be documented earlier than the late Eocene of Africa.

Oligocene primates from the Fayum, Egypt, show remarkable diversity. Twelve primates of five different taxonomic families have been described. Until recently, antecedents to these primates were unknown (*1*). Finds made in Egypt since 1987 of a second and different series of anthropoids from Eocene deposits give evidence about the roots of the anthropoid family tree. This second set of early higher primates comes from a site, locality 41 (L-41), situated north of Lake or "Birket" Qarun in the Jebel Qatrani Formation, Fayum Province, Egypt, which is dated at about 36 million years ago. The L-41 primates belong to seven different genera and species, one of which is undescribed (*2*–*4*). This brings the total of known Fayum primate species to 19. These Eocene species could belong to six or

---

Department of Biological Anthropology and Anatomy, Duke University, Durham, NC 27705-5000, USA.